Optical dielectric function of gold

Robert L. Olmon, Brian Slovick, Timothy W. Johnson, David Shelton, Sang-Hyun Oh, Glenn D. Boreman, and Markus B. Raschke

Phys. Rev. B **86**, 235147 — Published 28 December 2012

DOI: 10.1103/PhysRevB.86.235147

The optical dielectric function of gold

Robert L. Olmon[1], Brian Slovick[2], Timothy W. Johnson[3], David Shelton[2], Sang-Hyun Oh[3], Glenn D. Boreman[4], and Markus B. Raschke[1*]
[1] *Department of Physics, Department of Chemistry, and JILA, University of Colorado at Boulder, Colorado 80309, USA*
[2] *Center for Research and Education in Optics and Lasers (CREOL), University of Central Florida, Orlando, Florida 32816, USA*
[3] *Department of Electrical and Computer Engineering, University of Minnesota, Minneapolis, Minnesota 55455, USA and*
[4] *Department of Physics and Optical Science, University of North Carolina, Charlotte, North Carolina 28223, USA*

In metal optics gold assumes a special status because of its practical importance in opto-electronic and nano-optical devices, and its role as a model system for the study of the elementary electronic excitations that underlie the interaction of electromagnetic fields with metals. However, largely inconsistent values for the frequency dependence of the dielectric function describing the optical response of gold are found in the literature [1–3]. We performed precise spectroscopic ellipsometry measurements on evaporated gold, template-stripped gold, and single-crystal gold to determine the optical dielectric function across a broad spectral range of 300 nm – 25 μm (0.05 – 4.14 eV) with high spectral resolution. We fit the data to the Drude free-electron model, with an electron relaxation time $\tau_D = 14 \pm 3$ fs and plasma energy $\hbar\omega_p = 8.48$ eV. We find that the variation in dielectric functions for the different types of samples is small compared to the range of values reported in the literature. Our values, however, are comparable to the aggregate mean of the collection of previous measurements from over the past six decades. This suggests that although some variation can be attributed to surface morphology, the past measurements using different approaches seem to have been plagued more by systematic errors than previously assumed.

PACS numbers: 78.20.-e, 78.20.Ci, 78.30.Er

INTRODUCTION

The linear relative dielectric function of a homogeneous medium $\epsilon_r(\omega) = \epsilon_1(\omega) + i\epsilon_2(\omega)$ relates the electric field $\mathbf{E}(\mathbf{r},\omega)$ at position $\mathbf{r}$ (within the local approximation) with angular frequency ω to the displacement field $\mathbf{D}(\mathbf{r},\omega) = \epsilon_r(\omega)\epsilon_0\mathbf{E}(\mathbf{r},\omega)$ with ϵ_0 being the permittivity of free space [4]. In the absence of a magnetic response at optical frequencies, the dielectric function thus describes the aggregate response of electrons to incident light. ϵ_r is related to the electric susceptibility as $\chi(\omega) = 1 - \epsilon_r(\omega)$ and to the index of refraction as $\tilde{N}(\omega) = n(\omega) + ik(\omega) = \sqrt{\epsilon_r(\omega)}$. In metals, the complex conductivity $\sigma(\omega) = \sigma_1(\omega) + i\sigma_2(\omega) = -i\epsilon_0\omega(\epsilon_r(\omega) - 1)$ is of particular importance as the real part defines ohmic losses and the imaginary part is responsible for a phase offset between the local electric field and current density [4]. Knowledge of the dielectric function gives insight into fundamental electronic interactions in regular metals or strongly correlated electron systems, e.g. heavy-fermion compounds with high effective mass and resulting low electron relaxation rate [5].

At low energies, the optical dielectric function of monovalent metals like gold is associated with electronic intraband transitions within the conduction band. In this spectral range the optical response is dominated by free-electron behavior and provides information about the electron scattering rate and mean free path [4]. At higher energies, the optical dielectric function reflects the electronic interband transition from the occupied *d*-bands to the partially filled *sp* band. The energies of these transitions thus reveal insight into the electronic band structure.

Measurement of the optical frequency dependence of the dielectric function of gold has been the subject of several investigations over many years, motivated by the need to understand its fundamental electron behavior [1–3, 6–8]. Gold is also the metal of choice for a wide variety of optical and optoelectronic device applications due to its high optical conductivity and stability under ambient conditions. Precise knowledge of the frequency dependence of its dielectric function is required for successful nano-optical device engineering [9–12]. Resonant frequencies and spectral line widths of, e.g., plasmonic particles or optical antennas, nanoparticle coupling efficiency, surface plasmon excitation or propagation, and metamaterial properties all rely critically on the exact values of the optical dielectric function $\epsilon_r(\omega)$ of the materials and material combinations involved [9–15].

Here, we perform spectroscopic ellipsometry measurements on evaporated, template-stripped, and single-crystal optically thick gold surfaces to determine the optical dielectric function $\epsilon_r(\omega)$ across a broad spectral range from 0.05 eV to 4.14 eV (300 nm – 25 μm) with high spectral resolution. Fitting the free-electron model to our data below the onset of interband transitions, we give two free Drude parameters for each sample. Compared to the large variation among many previous measurements of the optical constants of gold, the optical dielectric functions of our three samples compare favorably despite the different surface morphologies. This suggests that besides sample preparation, the systematic errors and approximations in previous measurement methods may be more responsible for the differences between the measured optical dielectric functions than seems to have been previously realized.

Many past measurements have characterized the optical properties of gold. Figure 1 shows the spectral range and year of a selection of these measurements. For comparison our measurements are shown in blue. This list is not exhaustive, but it is representative of the methods used and the range of data extracted. In particular, we have focused on works where the data are available in tabulated form. A more comprehensive list of dozens of ϵ_r and $\tilde{N}$ measurements up to 1981 is listed with methods and energy ranges in [16]. Notably, the measurements of Thèye and Dold and Mecke are contained in a compilation by Lynch and Hunter, edited by Palik [17]. Several of the IR measurements in Fig. 1 were compiled and tabulated by Ordal et al. [3, 18].

Next we summarize the different experimental techniques, samples, and spectral ranges of several of the measurements shown in Fig. 1. Metal coated mica transmission interference filters and multiple reflections upon a glass-metal interface were used to measure n and k in the range 1.3 – 3.1 eV (400 – 950 nm) by Schulz and Tangherlini in 1954 [19, 20]. A temperature dependent reflectance measurement was conducted at $T = 82$ K and 295 K by Padalka and Shklyarevskii to determine n and k from 0.10 – 1.2 eV (1 – 12 μm) in 1961 [21]. A polarization method employing fourfold reflection in the range 0.13 – 0.50 eV (2.5 – 9.5 μm) on annealed gold samples was used to determine n and k by Bolotin et al. in 1962 [22]. The same method was used by Motulevich and Shubin in 1965 from 0.10 – 1.2 eV (1.0 – 12 μm) [23]. The index of refraction was measured using ellipsometry on evaporated gold on polished glass substrates in the IR from 0.089 eV – 0.992 eV (1.25 – 14 μm) by Dold and Mecke in 1965 [24]. The reflection coefficient was measured at normal incidence on a gold surface to obtain n and k in the IR in the range 0.04 – 0.4 eV (3 – 30 μm) by Bennett and Bennett in 1965 [25]. Reflection and transmission measurements were used to determine the index of refraction of evaporated semitransparent gold films of thickness 15 nm in the spectral range from 0.50 – 6.0 eV (210 nm – 2.48 μm) by Thèye in 1970 [6]. Similarly, the index of refraction of films with thicknesses 34 nm and 46 nm deposited onto fused-quartz substrates was measured by reflection and transmission from 0.50 – 6.5 eV (190 nm – 2.48 μm) by Johnson and Christy in 1972 [1, 26]. Transmission of IR light through a gold parallel plate waveguide

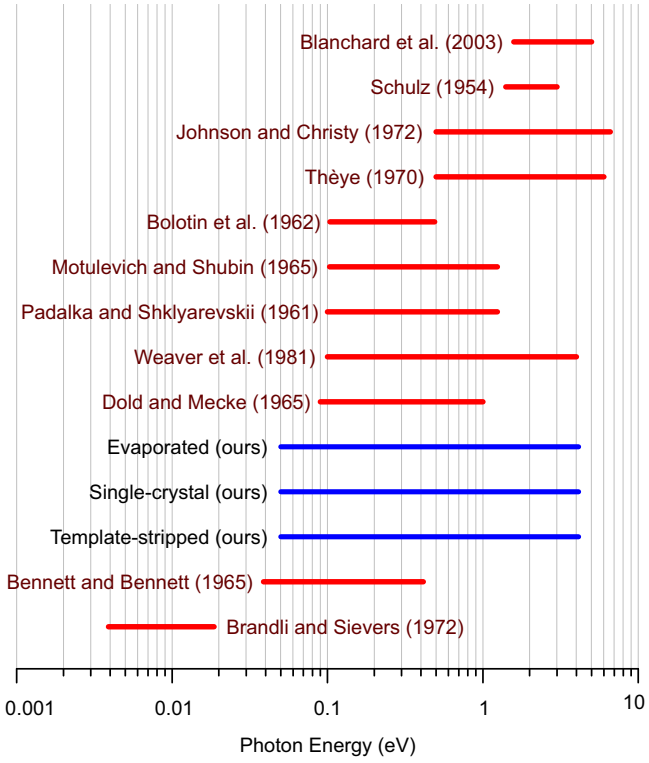

FIG. 1. Spectral range of several previous measurements of optical constants. Our measurements are indicated by the blue lines.

array was used to determine the surface resistance by Brandli and Sievers in 1972 [27], from which dielectric function values were calculated and tabulated by Ordal et al. from 3.90 – 18.6 meV (66.7 – 318 μm) [3]. The dielectric function of electropolished (110) gold at a temperature of 4.2 K was determined using Kramers-Kronig analysis on reflectance data measured from 0.1 – 4 eV (310 nm – 12.4 μm) by Weaver et al. in 1981 [16]. More recently in 2003 the complex permittivity of carefully cleaned (110) bulk single-crystal gold was measured in the 1.41 – 4.96 eV (250 – 850 nm) spectral range using spectroscopic ellipsometry [8].

A large variation in optical dielectric function values is found between these data sets. Known errors and anomalies make some of the data unusable [17]. In some cases the methodology is unclear or not specified in detail, which is particularly troublesome for compilations of original works that have become difficult to access [3]. Intricate measurements sometimes resulted in sparse data sets; significant interpolation or extrapolation is required to obtain the dielectric function at desired frequencies.

Increasingly sophisticated applications have prompted the need for more accurate data. Many device properties depend sensitively on the optical dielectric function. Here we list five such examples. 1) Raman scattering enhancement near a small metal nanoparticle with dielectric function $\epsilon = \epsilon_1 + i\epsilon_2$ in a medium with ϵ_m depends on $g = (\epsilon - \epsilon_m)/(\epsilon + 2\epsilon_m)$ to the fourth power, assuming the Stokes shift is considerably smaller than the resonance linewidth [28]. The Fröhlich resonance condition for the denominator of g, $\epsilon_1 = -2\epsilon_m$, is sensitive to the dielectric function with sensitivity governed by $d\epsilon_1(\omega)/d\omega$ in the region near resonance. For a free-electron metal, a deviation of 3% of ϵ_1 is enough to shift the polarizability of a 100 nm sphere in vacuum by half the linewidth. For gold, different experimental data reported for ϵ_1 in this range vary by about 8%. 2) The critical angle θ_c for total internal reflection depends nonlinearly on the optical dielectric functions of two interfacing materials, $\theta_c = \sin^{-1}(\sqrt{\epsilon_a/\epsilon_b})$ where a is the higher index material. θ_c is then especially sensitive when $\epsilon_a \approx \epsilon_b$. 3) The surface plasmon propagation length at the interface of a metal and a dielectric with ϵ_m is given by [13],

$$L_{spp} = \frac{c}{\omega}\left(\frac{\epsilon_1 + \epsilon_m}{\epsilon_1 \epsilon_m}\right)^{3/2} \frac{\epsilon_1^2}{\epsilon_2}, \tag{1}$$

Using dielectric function values from [6] vs. [16], the predicted L_{spp} varies by 50% at 1 eV, and 33% at 2 eV. 4) The

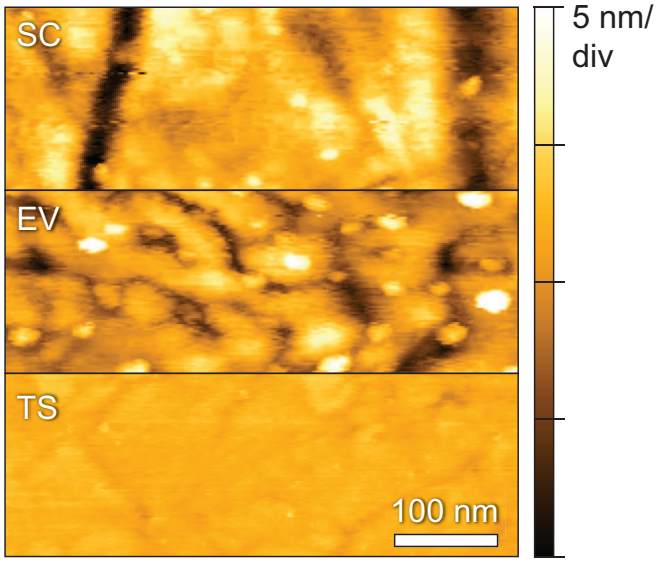

FIG. 2. Topography of single-crystal (SC), evaporated (EV), and template-stripped (TS) gold surfaces as measured with an atomic force microscope. Template-stripping significantly reduces the surface roughness compared to the evaporated sample.

Scattering linewidth of a noble metal nanoparticle, related to the plasmon dephasing time, exhibits a large sensitivity to the dielectric function, with a variation of up to 30% using different optical data in a finite difference time domain model ([6] vs. [1]) [29]. 5) The Casimir force between two nonideal gold plates depends in an intricate way on ϵ_2, and the expected Casimir force varies by up to 5% depending on the data set used to calculate it ([24] vs. [23]) [12].

EXPERIMENT

Previously the variation in the dielectric function of gold as measured by different groups has been largely attributed to sample preparation methods and surface morphology. Parameters such as surface roughness, grain size, void density, impurity density, film thickness etc. have been shown to affect the optical properties [1, 6, 30]. Indeed, differences in the visible region have been explained by void density alone [7]. Variations resulting from errors in differing measurement techniques, however, have been largely dismissed.

In order to investigate the role of surface preparation vs. measurement error, we measured the dielectric function of three types of gold samples: single-crystal Au(111) (SC, thickness 1 mm, diameter 10 mm, MaTecK GmbH), a 200 nm thick film deposited by evaporation onto a soda-lime glass substrate (EV), and a 200 nm thick template-stripped (TS) film deposited onto a clean silicon substrate in the same evaporation. The evaporation was conducted in an electron-beam evaporator (CHA Industries, Inc.) at a base pressure of 2.67×10^{-4} Pa, with an average rate of 0.6 nm/min. for the first 250 Å, then slowly increased to about 0.1 nm/s. To create the TS sample [31], after the gold was evaporated onto the silicon wafer, a drop of optical epoxy (Norland 61) was placed on the gold surface, and fixed to a soda-lime glass microscope slide. The epoxy was cured first under a UV lamp for 15 min., then on a hot plate set at 50 °C for 12 hours. The sample was then peeled off of the silicon, revealing the template-stripped surface.

The sample thickness in each case was chosen to significantly exceed the skin depth of gold ($\sim 20 - 45$ nm) for the entire wavelength range so that the measurements are representative of bulk behavior. When a metal film is thinner than the mean free path of the conduction electrons, the surface presents a significant boundary condition that must be accounted for [32]. As the thickness is reduced further, the surface gradually breaks up, with pit formation eventually leaving an array of metal islands on the substrate and producing corresponding changes in the optical properties. For films thicker than the electron mean free path in the bulk medium, the optical properties become largely independent of thickness, and represent those of the bulk [1, 32]. This occurs on evaporated gold films with thickness greater than about 25–30 nm.

Figure 2 shows the surface topography of the three samples as measured by dynamic atomic force microscopy (AFM, Innova, Bruker). Before performing the AFM measurements, each sample was rinsed in isopropanol and dried under nitrogen flow. The root mean square (rms) surface roughnesses of the SC, EV, and TS samples are $R_{rms} = 1.12$ nm,

1.26 nm, and 0.25 nm, respectively, in agreement with previous results [33]. The SC sample surface lacks crystal grain boundaries, but exhibits roughness on a lateral length scale of several hundred nanometers from the polishing process. As expected, template-stripping significantly reduces the roughness compared to the EV surface. The crystal grain size for the template-stripped surface is expected to be approximately the same size as for the evaporated surface, in the range of 10-70 nm.

For crystallite sizes equal in scale or smaller than the mean free path of the electrons, the electrons may experience scattering associated with the crystal boundaries. Annealing evaporated gold surfaces similar to ours has been shown to reduce both the real and imaginary parts of the dielectric function for 500 nm $< \lambda <$ 1000 nm, indicating lower damping due to larger crystal sizes and fewer grain boundary electron collisions [7, 34]. However, annealing has been known to roughen the surface in some cases, resulting in greater damping, especially in the IR where the longer mean free path means that the permittivity is more sensitive to the surface conditions [7]. We did not anneal our samples.

Template-stripping can alleviate some problems related to roughening. Annealing the film while it is still in contact with the template does not worsen the roughness, but only enlarges the grains, since the grains grow while being geometrically constrained by the smooth silicon template surface [31]. The effect of surface roughness and grain size for template-stripped films has been investigated previously by measuring the surface plasmon polariton propagation length on silver surfaces, with achieved propagation lengths approaching values predicted by theory for perfectly smooth homogeneous metal surfaces [31]. Gold template-stripped surfaces annealed at 550 °C then measured by ellipsometry have exhibited improved ϵ_2 and comparable ϵ_1 values compared to evaporated surfaces [35], indicating lower losses.

Ellipsometry compares the amplitude ratio $\tan\psi$ and phase difference $\Delta = \phi_p - \phi_s$ of the complex reflection coefficients r_s and r_p for s- and p-polarization components of the light at an oblique angle of incidence θ_i on the sample (i.e. $\rho = r_p/r_s = (\tan\psi)e^{i\Delta}$). The measured values ψ and Δ at θ_i are directly related to n and k at each wavelength investigated [36, 37]. Ellipsometry provides an advantage over other measurement techniques based on inversion of single angle reflectance R or transmittance T data to calculate n and k because it obviates ambiguities associated with Kramers-Kronig analysis. Kramers-Kronig analysis requires either measured or assumed data across a very broad spectral range for accurate determination of both the real and imaginary components of the optical parameters. This type of analysis may alternatively be avoided using inversion of reflection R and transmission T functions from multiple measurements. However, this inversion technique requires the selection of the intersection point of R and T contours in the n-k plane. This arbitrary designation can lead to a large uncertainty in n and k if the contours are nearly parallel, which tends to occur when either n or k is greater than 2 [1, 26]. Additionally, the transmission measurements require a thin sample with a well understood substrate optical response [1].

The complex frequency dependent dielectric function was measured on two variable angle spectroscopic ellipsometers (VASE and IR-VASE, J. A. Woollam Co.) with a rotating analyzer in the visible and a rotating compensator in the IR. The visible ellipsometer used here overcomes limitations associated with conventional rotating analyzer ellipsometers by employing a computer-controlled retardation element that allows for accurate measurements even near $\Delta = 0°$ or 180° as well as determination of the sense of rotation (i.e. handedness) of the light. Measurements were made for three angles of incidence $\theta_i = 65°$, 70°, and 80°. Ψ and Δ were measured for the photon energy region 0.620 eV to 4.13 eV distributed into 171 points (i.e., 300 nm to 2 μm with resolution of 10 nm) for the visible region, and 0.051 eV to 0.989 eV with steps of 4.0 meV for the IR region. The overlapping region from 0.62 eV to 0.99 eV was used to check consistency between the two instruments. The baseline of the instruments for transmission with no sample is better than $\delta\tan\Psi/\tan\Psi = 5\times10^{-3}$ and $\delta\cos(\Delta)/\cos(\Delta) = 1\times10^{-4}$ in the IR, and $\delta\tan\Psi/\tan\Psi = 1\times10^{-3}$ and $\delta\cos(\Delta)/\cos(\Delta) = 6\times10^{-6}$ in the visible according to manufacturer specifications.

The samples were assumed to be isotropic with negligible light depolarization upon reflection. The dielectric function of each sample was calculated based on a simple air-metal model. To ascertain the effects of possible systematic errors, we measured the permittivity of the three samples on two different spectroscopic ellipsometers in the visible regime (1.25 – 4.0 eV). In this range, the standard deviation between the two instruments was less than 0.18 and 0.15 for ϵ_1 and ϵ_2, respectively, with no discernible trend as a function of energy. Considering the small deviation, here we show our measured data only from the visible ellipsometer located in the same laboratory as the IR ellipsometer.

While we took great care to minimize any possible contamination during the measurements, it is difficult to completely avoid absorption of, e.g., water or organic impurities. Cleaning the samples by agitating them in isopropyl alcohol and drying them with nitrogen produced only minor changes in the measured dielectric functions, comparable to typical measurement-to-measurement variations. Even if a dielectric surface organic monolayer were present on the samples, we would expect the effect on the dielectric function to be minor compared to the bulk gold response due to the weak optical response of typical contaminants and the sheer volume of gold within the skin depth of $\delta \approx 25$ nm compared to the monolayer-scale thickness of a possible dielectric contamination layer. A dense overlayer, on the other hand, would produce a vibrational signature in the dielectric function, which was not observed.

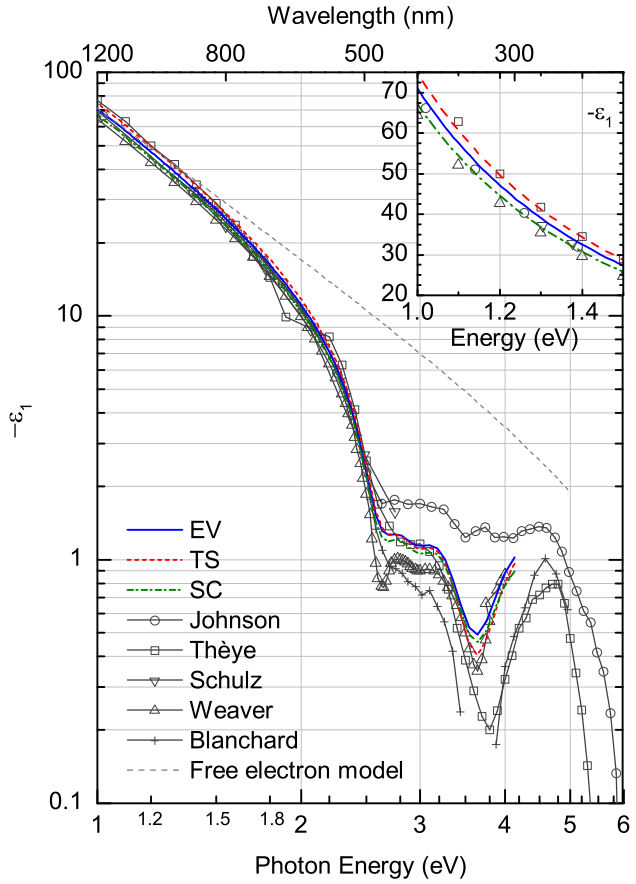

FIG. 3. (color online). Dielectric function of Au (negative real part $-\epsilon_1$) in the visible spectral region for our evaporated (EV), template-stripped (TS), and single-crystal (SC) gold samples. For comparison, data from Johnson and Christy (Johnson) [1], Thèye [6], Schulz [19, 20], Weaver et al. [16] and Blanchard et al. [8] are shown, as well as the dielectric function calculated for a Drude free-electron metal with $\hbar\omega_p = 8.48$ eV and $\tau_D = 14$ fs. Solid lines are guides for the eye. Inset: linear scale plot of $-\epsilon_1$ for 1.0 – 1.6 eV photon energy.

RESULTS

Figures 3 and 4 show the negative of the real part of the dielectric function $-\epsilon_1$ and the imaginary part ϵ_2, respectively, of the evaporated (EV, blue solid line), template-stripped (TS, red dashed), and single-crystal (SC, green dot-dashed) samples in the energy range 1 eV $< E <$ 6 eV. For comparison, data from Johnson and Christy [1] (circles), Thèye [6] (squares, from tabulated data in [2]), Schulz [19, 20] (down-triangle), Weaver et al. [16] (up-triangle), and Blanchard et al. [8] (crosses) are plotted. The thin gray dashed line shows the dielectric function calculated for a Drude free electron metal with $\hbar\omega_p = 8.48$ eV and $\Gamma = 0.0484$ eV, as discussed below. Lines connecting the data points are guides for the eye. The inset in Fig. 3 shows the same data on a linear scale in a reduced spectral range from 1.0 to 1.6 eV.

Corresponding data for the IR spectral range for $-\epsilon_1$ and ϵ_2 are shown in figs. 5 and 6, respectively. For comparison, data are shown from Johnson and Christy [1] (circles), Dold and Mecke [24] (square, from tabulated data in [2]), Bennett and Bennett [25] (pentagon), Bolotin et al. [22] (left-triangles), Motulevich and Shubin [23] (down-triangle), Padalka and Shklyarevskii [21] (diamond), and Weaver et al. [16] (up-triangle). In the region of spectral overlap of the UV/vis and IR ellipsometers, between 0.62 eV and 0.99 eV (1.3 – 2.0 μm) we plot the mean of the dielectric function values weighted as a percentage by the proximity to the edge of the measurement range of each instrument. The optical dielectric function for a free electron metal with Drude parameters $\hbar\omega_p = 8.48$ eV and $\Gamma = 0.0484$ eV is also plotted (dashed thin line).

Within the *Drude-Sommerfeld free electron model*, noble metals are described as a gas of noninteracting electrons with a frequency dependent dielectric function. The dielectric function $\epsilon_r(\omega)$ is derived by solving the equation of

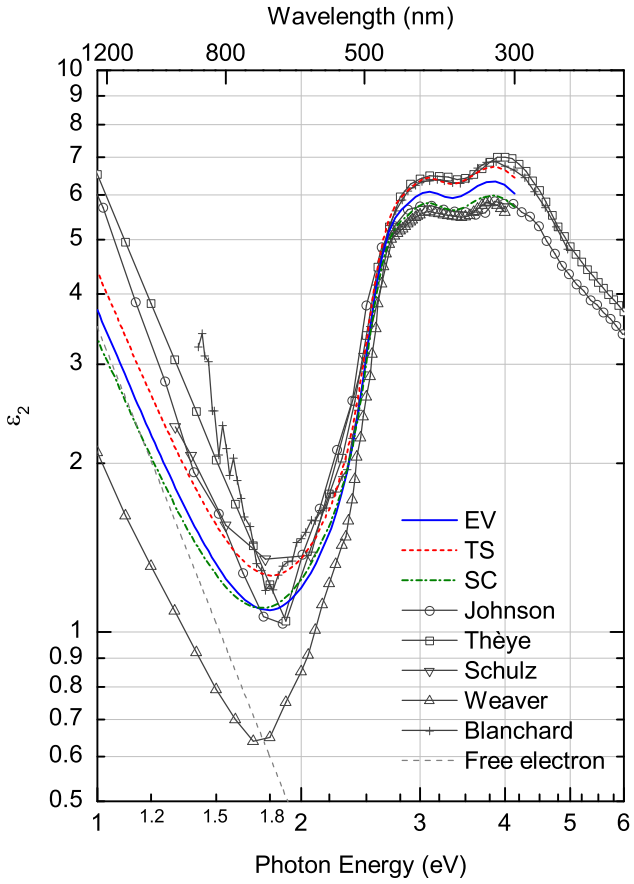

FIG. 4. (color online). Dielectric function of Au (imaginary part ϵ_2) in the visible spectral region for evaporated (EV), template-stripped (TS), and single-crystal (SC) gold samples. For comparison, data from Johnson and Christy (Johnson) [1], Thèye [6], Schulz [19, 20], Weaver et al. [16], and Blanchard et al. [8] are shown, as well as the dielectric function calculated for a Drude free electron metal with $\hbar\omega_p = 8.48$ eV and $\tau_D = 14$ fs.

motion for the electrons driven by a time-harmonic electric field with an effective electron relaxation time τ_D [4]. The solution is similar to that of a damped harmonic oscillator, but with no restoring force, i.e. resonance at $\omega = 0$ s^{-1} [38] (Drude peak). $\epsilon_r(\omega)$ is then given by

$$\epsilon_r(\omega) = \epsilon_1(\omega) + i\epsilon_2(\omega) = 1 - \frac{\omega_p^2}{\omega^2 + i\Gamma\omega}, \tag{2}$$

with $\Gamma = 1/\tau_D$ the electron relaxation rate, $\omega_p = (Ne^2/\epsilon_0 m^*)^{1/2}$ the plasma frequency, N the number of electrons per unit volume, $e = 1.602 \times 10^{-19}$ C the electron charge, $\epsilon_0 = 8.854 \times 10^{-12}$ F/m the permittivity of free space, and m^* the effective mass of the electron. As the mean free time between electron scattering events within the free electron model, the relaxation time τ_D parameterizes the cumulative effects of various electron scattering processes. The relaxation rate has contributions from electron-electron scattering, temperature-dependent electron-phonon scattering, scattering at grain boundaries, impurity and defect scattering, and surface roughness scattering contributions [39, 40]. The parameters Γ and ω_p can be extracted from a fit to the experimental data, as discussed below. While this phenomenological model does not provide physical insight into the damping mechanism itself, it nevertheless describes the relationship between the permittivity and the collective electron response in the low-frequency region dominated by the free carrier response of gold.

To obtain the Drude parameters ω_p and Γ, we fit our data to Eq. 2 using a so-called simulated annealing algorithm [41]. The recovered parameters represent the fit with the least error for $\epsilon_1(\omega)$ and $\epsilon_2(\omega)$ simultaneously. The fitted parameters for the EV, TS, and SC samples are $\hbar\omega_p = 8.5 \pm 0.5$ eV, 8.80 ± 0.05 eV, and 8.1 ± 0.8 eV; and $\tau_D = 1/\Gamma = 14 \pm 3$ fs, 13 ± 1 fs, and 14 ± 4 fs, respectively. The error is calculated based on variation of ω_p and Γ parameters when the real and imaginary parts are fitted separately.

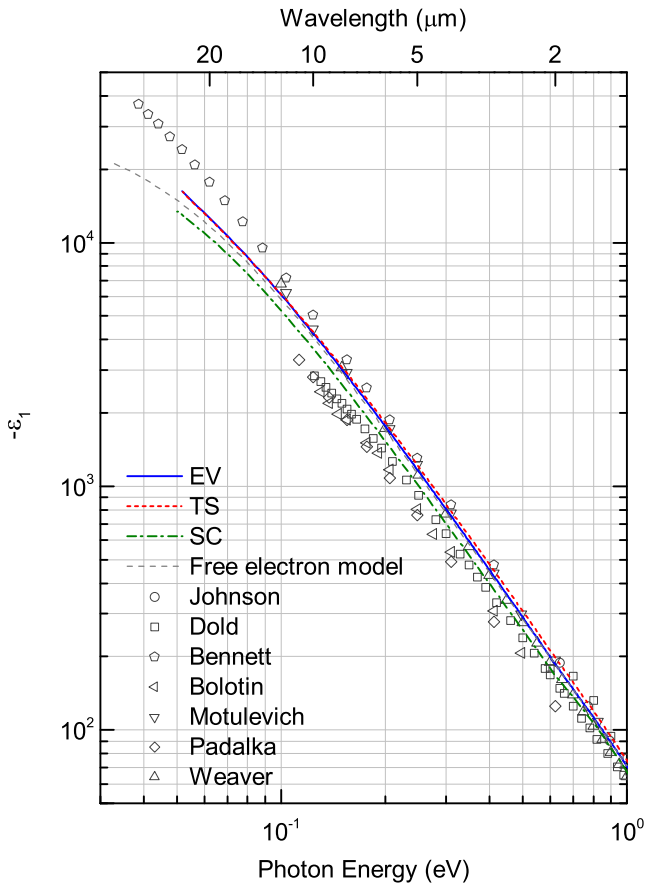

FIG. 5. (color online). Permittivity of Au (negative real part $-\epsilon_1$) in the IR spectral region for evaporated (EV), template-stripped (TS), and single-crystal (SC) samples. Data from Refs. [1, 16, 21–25, 27], and the calculated Drude free electron model with $\hbar\omega_p = 8.48$ eV and $\tau_D = 14$ fs are also shown for comparison.

An alternative approach, based on the following approximation, results in nearly identical fit values. For $\omega \gg \Gamma$, but below the onset of the interband response, the Drude dielectric function reduces to

$$-\epsilon_1 \approx \frac{\lambda^2}{\lambda_p^2} - 1, \text{and} \tag{3}$$

$$\epsilon_2 \approx \Gamma \frac{\lambda^3}{2\pi c \lambda_p^2}, \tag{4}$$

with $\lambda_p = 2\pi c/\omega_p$. Equation 3 is used to find ω_p by the slope of $-\epsilon_1$ vs. λ^2, and Eq. 4 is used to find Γ by the slope of ϵ_2 vs. λ^3. Using this approach from 0.5 to 1.0 eV ($\lambda = 1.24$ to 2.48 μm), τ_D is obtained as 15 fs, 14 fs, and 12 fs, for EV, TS, and SC, and $\hbar\omega_p$ as 8.5 eV, 8.8 eV, and 7.9 eV, respectively, in good agreement with the values determined above. The mean values for our three samples are $\hbar\omega_p = 8.45 \pm 0.44$ eV, $\tau_D = 14 \pm 3$ fs. The dielectric function from the free-electron model using these parameters is plotted in Figs. 3 – 6 (thin gray dashed line).

DISCUSSION

In the *visible spectral region*, the measured dielectric function data fall within the range of other measurements from literature. The real part of the optical dielectric function shown in Fig. 3 exhibits the greatest relative variation in the interband region, $E > 2.5$ eV. At high energy, the magnitudes of the measured values are significantly less than those of Johnson and greater than those of Thèye and Blanchard. Johnson and Christy have attributed their higher $|\epsilon_1|$ to their thicker, bulk-like film compared to Thèye's 15 nm thick film [1]. However, our data agree better with

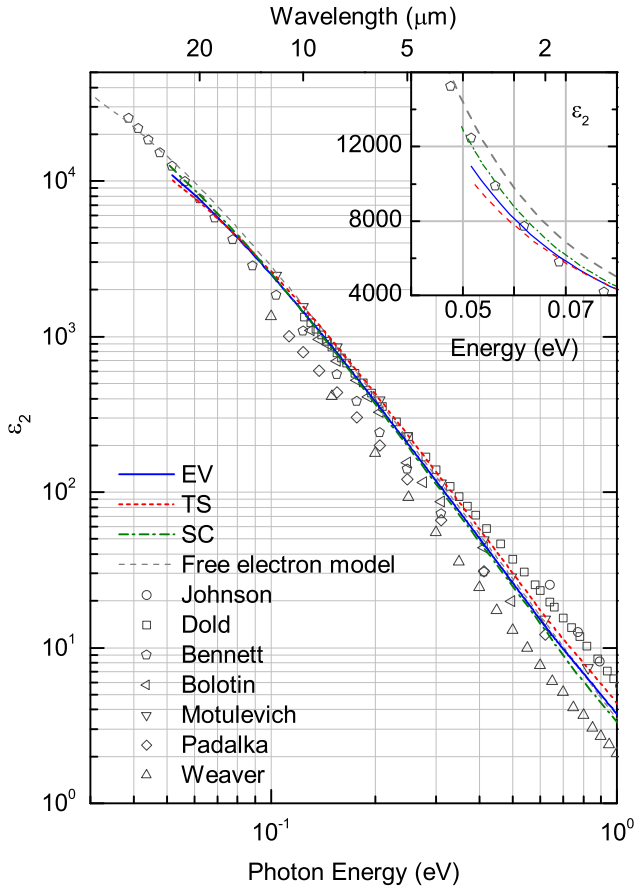

FIG. 6. (color online). Permittivity of Au (imaginary part ϵ_2) in the IR spectral region for evaporated (EV), template-stripped (TS), and single-crystal (SC) samples. Data from Refs. [1, 16, 21–25, 27] and the calculated Drude free electron model with $\hbar\omega_p = 8.48$ eV and $\tau_D = 14$ fs are also shown for comparison. For energy between the interband region and $\sim \Gamma$, higher ϵ_2 corresponds to higher damping (lower τ_D), indicating that $\tau_{D,TS} < \tau_{D,EV} < \tau_{D,SC}$. Near $E < \Gamma$, the order of the ϵ_2 curves reverses (inset).

Thèye's data up to about 3.5 eV despite our thicker bulk-like films, and despite different preparation methods. One notable exception occurs near 2 eV in Thèye's data, where one would expect a smoother increase in $|\epsilon_1|$ toward lower energy.

Fig. 4 shows the imaginary component ϵ_2 in the visible range. Two distinct regions can be seen, divided at about 1.8 eV, corresponding to the interband absorption edge. At higher energy, our data are bounded on each side by the data from the literature. At lower energy all three of our measured samples exhibit lower ϵ_2 compared to the data of Johnson, Thèye, Schulz, and Blanchard. The data of Weaver are yet lower by nearly a factor of 2 compared to the TS data. The data from Weaver are included to illustrate some of the effects of cryogenic temperatures on the optical dielectric function, as those data were measured at 4.2 K [16]. Temperature effects will be discussed in greater detail below. Our results agree with related measurements on similar samples in the visible [42, 43].

In the visible spectral region, the optical response is dominated by interband transitions from the *d*-bands to the *sp* band that crosses the Fermi level with a theoretical transition band edge at 2.5 eV [6, 7]. The associated absorption tail extends to about 1.8 eV (see Fig. 4) [6, 7], limiting the applicability of the free electron model to photon energies $E \lesssim 1.8$ eV. The model description of the optical response can be extended into the interband region by empirically adding parameterized Lorentz or Gaussian oscillators to Eq. 2 to account for resonant absorption [11, 29] which we do not pursue here.

Differences in ϵ_2 in the interband region $E > 1.8$ eV can be attributed to differing effective volume densities of voids in the interaction region, where the voids correspond to either surface roughness or contamination layers [7]. The void fraction alone, without contributions from strain or scattering at defects or grain boundaries is enough to explain the differences in this spectral region, with a single-parameter effective medium model accounting for a change

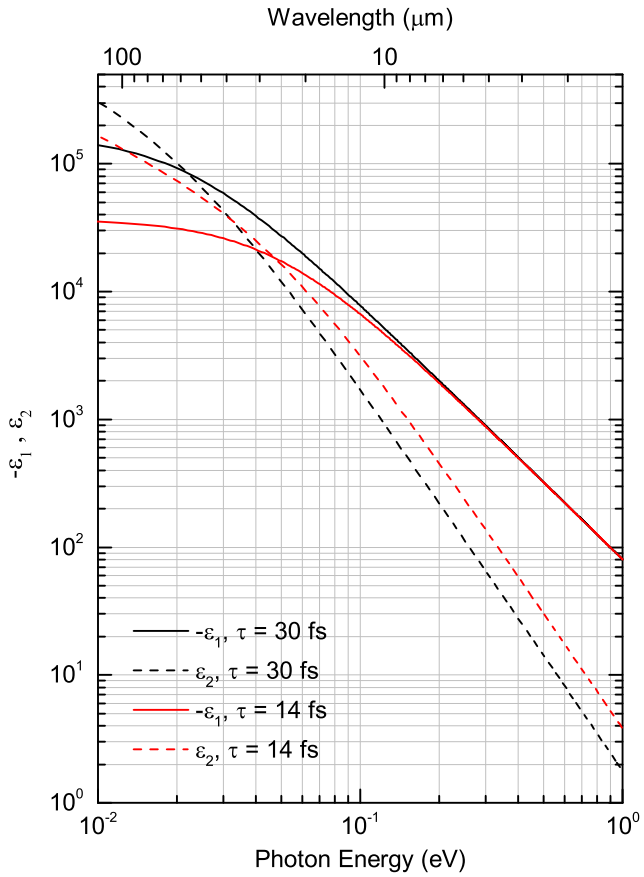

FIG. 7. Calculated dielectric function $\epsilon_r(\hbar\omega) = \epsilon_1(\hbar\omega) + i\epsilon_2(\hbar\omega)$ for $\tau_D = 14$ fs (red) and 30 fs (black). Larger values of τ_D result in higher $|\epsilon_1|$ and ϵ_2 at low photon energies with a higher sensitivity for $|\epsilon_1|$; and with *lower* ϵ_2 at intermediate energies of 0.1∼1.0 eV, where $|\epsilon_1|$ does not depend significantly on τ_D.

in overall magnitude, but not the spectral shape of ϵ_2. According to this model, higher ϵ_2 values in the visible regime correspond to lower effective void density. The TS surface has a higher ϵ_2 than the EV surface due to lower surface roughness for TS. The SC surface has the lowest ϵ_2, due to roughness resulting from polishing (see Fig. 2). We note here that sometimes in the context of a multilayer surface model, the term pseudodielectric function is used to refer to the dielectric function of combined pure bulk layers and interfacial layers [37], but we retain the term dielectric function for the combined response for consistency with the established literature.

In the *IR region* our ϵ_1 and ϵ_2 data fall within the broad range of previous literature values (see Figs. 5 and 6). Our EV and TS ϵ_1 data agree well throughout the entire spectral range, with the best agreement at lower energy. In comparison, our SC data have a consistently lower $|\epsilon_1|$. For ϵ_2 we observe that samples with higher ϵ_2 at 1 eV have lower ϵ_2 at 0.05 eV as seen for our EV, TS, SC, and results from Bennett. Lynch and Hunter note that the data from Dold and Mecke may contain erroneously low k values at longer wavelengths, but they nevertheless included them in their compilation [17].

With regard to $\tau_D = 14 \pm 3$ fs and $\hbar\omega_p = 8.45 \pm 0.44$ eV extracted from our data, in comparison, Johnson and Christy find $\tau_D = 9$ fs and $\hbar\omega_p = 9.06$ eV [1]. Bennett and Bennett obtain $\tau_D = 25$ fs (they assume $\hbar\omega_p = 9.0186$ eV calculated from the electron rest mass) [25]. A parameterized fit to the data from Dold and Mecke [24] and Thèye [6] yields $\tau_D = 12.4$ fs and $\hbar\omega_p = 7.86$ eV [11]. Interestingly, the parameters extracted from a fit to the aggregated data from all other works plotted in Figs. 3–6 are $\hbar\omega_p \simeq 8.48$ eV and $\tau_D \simeq 14$ fs, in good comparison with our data.

Figure 7 shows the spectral dependence of the real and imaginary parts of the dielectric function on τ_D for a free-electron metal in the energy range 0.01 eV – 1 eV. Two different relaxation times are compared: 14 fs (red), corresponding to a fit to our data, and 30 fs (black), as calculated from DC conductivity measurements of gold [44]. For the plasma frequency $\hbar\omega_p = 9.0186$ eV is used, as calculated assuming $m^* = m_e$, where $m_e = 9.11 \times 10^{-31}$ kg is

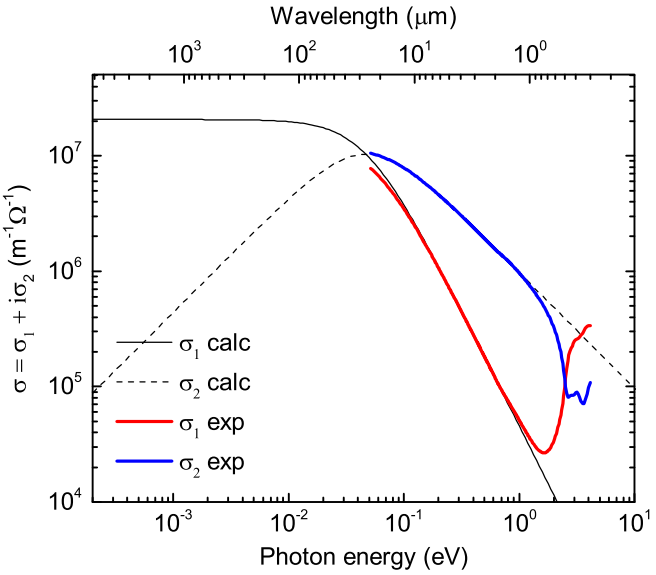

FIG. 8. The mean complex conductivity $\sigma(\hbar\omega) = \sigma_1(\hbar\omega) + i\sigma_2(\hbar\omega)$ of the EV, SC, and TS samples. For comparison, $\sigma_1(\hbar\omega)$ (solid line) and $\sigma_2(\hbar\omega)$ (dashed line) derived from the Drude-Sommerfeld free-electron model ($\tau_D = 14$ fs and $\hbar\omega_p = 8.48$ eV) are shown.

the electron rest mass. Near the frequency $\omega = \Gamma$, the absolute values of the real and imaginary parts of the dielectric function cross, $|\epsilon_1| = \epsilon_2$. For photon energies above this crossover point, a lower τ_D (i.e. more frequent collisions, and thus more damping) is associated with an *increase* of ϵ_2, while below this point, a lower τ_D results in a *decrease* in both $|\epsilon_1|$ and ϵ_2.

Assuming ideal Drude behavior, systematic variations of dielectric function values in different ranges could allow one to make conclusions about the electron damping on different types of samples by comparing the data to the model as seen in Fig. 7. For example, it may be possible to distill the relative contributions of surface roughness vs. crystal grain size on damping. Indeed, with a mean grain diameter of approximately 40 nm, and electron mean free path calculated from our data of $l = v_f\tau_D$ of about 20 nm, where $v_f = 1.40 \times 10^8$ cm/s is the Fermi velocity for gold [44], field-induced surface parallel drift of electrons is expected to result in a significant collision rate with grain boundaries. However, the slight deviation of our data from perfect Drude behavior prevents us from making fine conclusions about the relative contributions of damping mechanisms in this way.

Broad trends related to damping can be seen, however. According to the trend in ϵ_2 in Fig. 7, lower damping is seen in the Bennett, Bolotin, Padalka, and Weaver data compared to the SC, EV, and TS samples. Bennett additionally exhibits a knee or rolloff at lower energy compared to our data, as expected for lower damping. The slopes of our data, and those of Weaver and Thèye near $E = 1$ eV (Fig. 4) are similar, while those of Johnson and Blanchard deviate significantly. This suggests that the Johnson and Blanchard data deviate from the free electron behavior, as according to Fig. 7, the slope should not depend on τ_D in that energy range.

In the IR, damping is also dependent on temperature due to a decrease in phonon excitation density at low temperatures and a corresponding decrease in the rate of electron-phonon collisions [21, 39, 45]. While we do not study effects of temperature here, they can be great and should be noted. Decreasing the temperature from $T = 295$ K to 82 K, the electron-phonon collision frequency decreases from 1.94×10^{13} s^{-1} to 0.74×10^{13} s^{-1} [21]. Index of refraction n values at 295 K were found to be 1.27 ± 0.07 times greater than those measured at 82 K from 1 – 11 μm. k was found to have a much smaller temperature dependence, with negligible change from 1 μm to 6 μm, and a 3% increase at 11 μm. The data from Weaver [16], measured at 4.2 K, have the lowest ϵ_2 in the intraband region, reflecting the decreased electron-phonon damping rate (see Figs. 4 and 6).

Figure 8 shows the derived mean *complex conductivity* $\sigma(\omega) = \sigma_1(\omega) + i\sigma_2(\omega)$ of the EV, SC, and TS samples compared to that derived from the Drude-Sommerfeld free-electron model, real part (solid line) and imaginary part (dashed line), with $\tau_D = 14$ fs, and $\hbar\omega_p = 8.48$ eV. The crossover point between σ_1 and σ_2 occurs at radial frequency $E/\hbar = \Gamma = 1/\tau_D$. The mid- to near-IR spectral range is characterized by a significantly reduced real part, and high imaginary part compared to lower (near DC) frequencies. This is associated with greater ohmic damping and a large phase offset between the excitation field and the charge motion [4].

The average *effective mass* of the conduction electrons within the Drude model is related to the plasma frequency

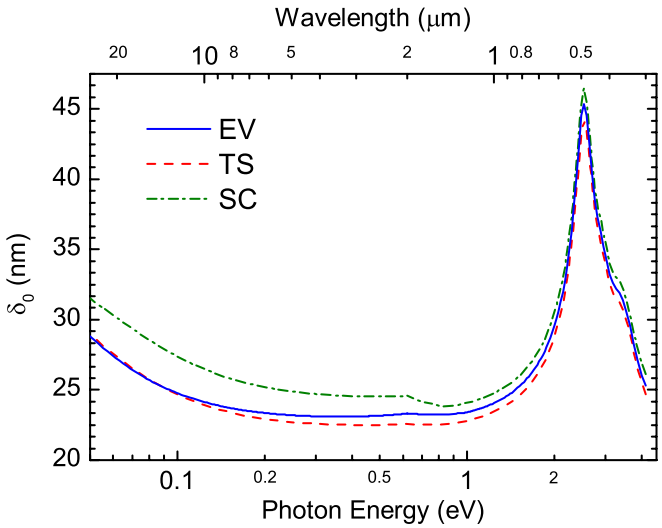

FIG. 9. The skin depth δ_0 vs. photon energy for our three samples as calculated from dielectric function data. The skin depth is particularly sensitive to the dielectric function.

as $m^* = Ne^2/\epsilon_0\omega_p^2$. ω_p specifies the ratio N/m^*. Following the common assumption of one conduction electron per atom contributing to the optical response, i.e., $N = 5.9 \times 10^{22}$ cm^{-3} for gold, we obtain for the evaporated, template-stripped, and single-crystal samples, m^*/m_e of 1.12, 1.06, and 1.31, respectively.

The normalized effective mass m^*/m_e as determined by other measurements varies significantly as shown in Table I. This variation has been noted previously for over-annealed surfaces that may contain voids and thus have a lower average density of conduction electrons [6]. However, assuming N is fixed, the effect of void space is seen through m^*. By this argument, rough surfaces should have a lower mean conduction electron density compared to smooth ones, as reflected in a larger value for m^*. Indeed the TS gold, the smoothest of our three samples, has the lowest effective mass.

An electromagnetic wave experiences attenuation as it penetrates into an absorptive medium. The distance into the medium at which the electric field amplitude is $1/e$ times the amplitude at the surface is known as the *skin depth* and is given by $\delta_0 = c/\omega k$. Figure 9 shows δ_0 as a function of photon energy for our three samples. From this graph it is apparent that the skin depth is very sensitive to the exact values of the dielectric function. The kink in the SC data near 0.65 eV is due to the small measurement difference between the visible and IR ellipsometers. Notably, the skin depth is nearly constant with a value of $\delta_0 \approx 25$ nm throughout the near- to mid-IR (i.e., in the range 1 μm – 10 μm). This is a result of the fact that in this spectral region the attenuation constant k decreases at the same rate that the frequency ω increases. The SC data exhibit a somewhat longer δ_0 compared to the EV and TS data. Since

$$k^2 = \frac{\sqrt{\epsilon_1^2 + \epsilon_2^2} - \epsilon_1}{2}, \tag{5}$$

the greater skin depth for the SC sample is consistent with the lower $|\epsilon_1|$ and ϵ_2 values that we measure for the SC sample in this range.

The variation in optical dielectric function values between our EV, TS, and SC samples is significantly less than the variation in the literature through most of the spectrum. This suggests that the variations cannot be explained

TABLE I. Normalized Effective Electron Mass

Sample	m^*/m_e
EV	1.12
TS	1.06
SC	1.31
Theye [6]	0.94
Johnson and Christy [1]	0.99
Parkins et al. [46]	1.08
Rakic et al. [11]	1.32
Svetovoy et al. [30]	1.75

by differing sample preparation methods alone. Systematic errors in the different measurement techniques employed may be the primary factor. The good agreement between the expected Drude model behavior and our data and the data of many previous measurements indicates that our data contain relatively few systematic errors.

SUMMARY

In conclusion, we have measured the optical dielectric function of gold across a broad spectral range from 0.05 – 4.14 eV for optically thick evaporated, template-stripped, and single-crystal surfaces. We find only small variations in values between these different types of samples. This suggests that the exact value of the dielectric function is considerably less sensitive to sample morphology and preparation, in contrast to previous interpretations of the large apparent variations between the different values reported in the literature. This indicates that many of the previous measurements have been plagued by systematic errors and too coarse assumptions underlying some of the more indirect procedures applied which led to either an over or underestimate of the dielectric function values deduced. While comparison suggests that our precise measurements surpass many of those of the past six decades in accuracy, this can only be verified through their use over time to model optical phenomena that are sensitive to the exact value of the dielectric function. The dielectric function data from our measurements may be obtained as supplementary material, or downloaded from our group website: `http://nano-optics.colorado.edu`.

ACKNOWLEDGEMENTS

We would like to thank Dr. Joachim Krenn, Dr. Bruno Gompf, and Dr. Paul Ashby for illuminating discussions. Funding from the National Science Foundation (NSF CAREER grant CHE0748226 and grant ECCS-1204993) is gratefully acknowledged.

* markus.raschke@colorado.edu

[1] P. B. Johnson and R. W. Christy, Physical Review B **6**, 4370 (1972).
[2] E. D. Palik, ed., *Handbook of Optical Constants of Solids* (Academic Press, Inc., 1998).
[3] M. A. Ordal, L. L. Long, R. J. Bell, S. E. Bell, R. R. Bell, R. W. Alexander, and C. A. Ward, Appl. Opt. **22**, 1099 (1983).
[4] M. Dressel and G. Grüner, *Electrodynamics of Solids* (Cambridge University Press, 2002).
[5] M. Scheffler, M. Dressel, M. Jourdan, and H. Adrian, Nature **438**, 1135 (2005).
[6] M.-L. Thèye, Phys. Rev. B **2**, 3060 (1970).
[7] D. E. Aspnes, E. Kinsbron, and D. D. Bacon, Phys. Rev. B **21**, 21 (1980).
[8] N. P. Blanchard, C. Smith, D. S. Martin, D. J. Hayton, T. E. Jenkins, and P. Weightman, Phys. stat. sol. (c) **0**, 2931 (2003).
[9] A. Trügler, J.-C. Tinguely, J. Krenn, A. Hohenau, and U. Hohenester, Phys. Rev. B **83**, 081412 (2011).
[10] P. Berini, R. Charbonneau, N. Lahoud, and G. Mattiussi, J. Appl. Phys. **98**, 043109 (2005).
[11] A. D. Rakić, A. B. Djurišić, J. M. Elazar, and M. L. Majewski, Appl. Opt. **37**, 5271 (1998).
[12] I. Pirozhenko, A. Lambrecht, and V. B. Svetovoy, New J. Phys. **8**, 238 (2006).
[13] H. Raether, *Surface plasmons on smooth and rough surfaces and on gratings* (Springer-Verlag, 1988).
[14] W. L. Barnes, J. Opt. A: Pure Appl. Opt. **11**, 114002 (2009).
[15] D. Canchal-Arias and P. Dawson, Surface Science **577**, 95 (2005).
[16] J. H. Weaver, C. Krafka, D. W. Lynch, and E. E. Koch, *Optical properties of metals, Pt. II* (Fachinformationszentrum Energie, Physik, Mathematik, 1981).
[17] D. W. Lynch and W. R. Hunter, in *Handbook of Optical Constants of Solids*, edited by E. D. Palik (Academic, San Diego, 1998), vol. 1.
[18] Note that Ordal tabulates data from Weaver et al. [16], but significantly abbreviates it, and neglects to mention the measurement temperature of $T = 4.2$ K. The data used for comparison in the present work are taken from the original sources when possible.
[19] L. G. Schulz, J. Opt. Soc. Am. **44**, 357 (1954).
[20] L. G. Schulz and F. R. Tangherlini, J. Opt. Soc. Am. **44**, 362 (1954).
[21] V. G. Padalka and I. N. Shklyarevskii, Opt. spectrosc. **11**, 285 (1961).
[22] G. A. Bolotin, A. N. Voloshinskii, M. M. Neskov, A. V. Sokolov, and B. A. Charikov, Phys. Met. and Metallogr. **13**, 823 (1962).
[23] G. P. Motulevich and A. A. Shubin, Soviet Phys. JETP **20**, 560 (1965).
[24] B. Dold and R. Mecke, Optik **22**, 435 (1965).
[25] H. E. Bennett and J. M. Bennett, in *Colloquium on the Optical Properties and Electronic Structure of Metals and Alloys*, edited by F. Abeles (North-Holland, Amsterdam, Paris, France, 1965), p. 175.
[26] J. E. Nestell and R. W. Christy, Appl. Opt. **11**, 643 (1972).
[27] G. Brandli and A. J. Sievers, Phys. Rev. B **5**, 3550 (1972).
[28] P. L. Stiles, J. A. Dieringer, N. C. Shah, and R. P. Van Duyne, Annu. Rev. Anal. Chem. **1**, 601 (2008).
[29] K. Munechika, J. Smith, Y. Chen, and D. Ginger, J. Phys. Chem. C **111**, 18906 (2007).
[30] V. B. Svetovoy, Phys. Rev. B **77**, 035439 (2008).
[31] P. Nagpal, N. C. Lindquist, S.-H. Oh, and D. J. Norris, Science (New York, N.Y.) **325**, 594 (2009).
[32] C. Reale, Infrared Phys. **10**, 175 (1970).
[33] P. Nagpal, N. C. Lindquist, S.-H. Oh, and D. J. Norris, Supplement to: Science (New York, N.Y.) **325**, 594 (2009).
[34] J.-C. Tinguely, I. Sow, C. Leiner, J. Grand, A. Hohenau, N. Felidj, J. Aubard, and J. R. Krenn, Bionanoscience **1**, 128 (2011).
[35] D. J. Norris, *Private communication* (2012).
[36] D. E. Aspnes, in *Handbook of Optical Constants of Solids, Vol. 1*, edited by E. D. Palik (Academic Press, Inc., San Diego, CA, 1998), 2, chap. 5, pp. 89–112.
[37] J. Humlíček, in *Handbook of Ellipsometry*, edited by H. G. Tompkins and E. A. Irene (William Andrew, Inc., 2005).
[38] G. R. Fowles, *Introduction to Modern Optics* (Dover, 1989).
[39] M. Liu, M. Pelton, and P. Guyot-Sionnest, Phys. Rev. B **79**, 035418 (2009).
[40] P. Wissman and H.-U. Finzel, *Electrical Resistivity of Thin Metal Films* (Springer, 2007).
[41] Simulated annealing was done in Matlab using the *anneal* function, referencing S. Kirkpatrick, C. D. Gelatt, and M. P. Vecchi, Science, **220**, 671-680 (1983).
[42] B. Gompf, *Private communication* (2012).
[43] J. Krenn, *Private communication* (2011).
[44] N. W. Ashcroft and N. D. Mermin, *Solid State Physics* (Harcourt, Inc., 1976).
[45] G. Cisneros and J. S. Helman, Phys. Rev. B **25**, 6504 (1982).
[46] G. R. Parkins, W. E. Lawrence, and R. W. Christy, Physical Review B **23**, 6408 (1981).